

DAA/ LANGLEY  
NAG 1-441

IN-36

63685  
42P

## Semiannual Progress Report

Submitted to: National Aeronautics and  
Space Administration  
Langley Research Center  
Hampton, Va 23665

Institution: Hampton University  
Dept of Physics and Engineering

Title of Research: Direct Solar-Pumped Iodine Laser  
Amplifier

NASA Grant Number NAG-1-441

Period Covered March 1, 1986 - Aug 31, 1986

Principal Investigator Dr. Kwang S. Han

Research Associates Dr. K. H. Kim  
Mr. L. V. Stock

(NASA-CR-180296) DIRECT SLAB-PUMPED IODINE  
LASER AMPLIFIER Semiannual Progress Report,  
1 Mar. - 31 Aug. 1986 (Hampton Inst.) 42 p  
Avail: NTIS HC A03/MF A01 CSCL 20E

N87-26328

Unclas  
G3/36 0063685

# Direct Solar-Pumped Iodine Laser Amplifier

## Contents

Abstract	i
I. Feasibility study of solar-pumped dye laser	
A. Introduction	1
B. Experiment	2
C. Summary and conclusion	5
D. List of figures	6
E. Appendix	16
F. References	18
II. Kinetic Modeling of the Solar-Pumped Iodine Laser	
A. Introduction and results	19
B. List of figures and tables.	22

## Abstract

This semiannual progress report covers the period from March 1, 1986 to Aug 31, 1986 under NASA grant NAG-1-441 entitled "Direct solar-pumped iodine laser amplifier". During this period the feasibility study of solar-pumped dye lasers and the kinetic modeling of a solar-pumped iodine laser amplifier have been carried out.

In order to evaluate the feasibility of the solar-pumped dye laser, the parametric study of a dye laser amplifier pumped by a solar-simulator and flashlamp was carried out, and the amplifier gains were measured at various pump-beam irradiances on the dye cell. Rhodamine 6G was considered as a candidate for the solar-pumped laser because of its good utilization of the solar spectrum and high quantum efficiency. The measurement shows that a solar concentration of 20,000 is required to reach the threshold of the dye at present time.

The work to construct a kinetic model algorithm which predicts the output parameters of laser (lasing time, time to threshold, and pulse energy) has been progressed. To this date the kinetic model has been improved such that there is good agreement between the theoretical model and experimental data for the systems defined in the previous progress reports as flashlamp-pumped laser oscillator, and the long path-length solar-pumped laser. Both experimental data sets are for the lasing  $i\text{-C}_3\text{F}_7\text{I}$  whose reaction ratios are well known as compared with the other iodide. Since the results of the fit for this relatively well known gas are qualified, the other gases and their subsequent kinetic rates can be studied with greater confidence.

## I. Feasibility Study of solar-pumped dye lasers

### A. Introduction

Liquid dye lasers have many desirable characteristics for solar pumping. They have absorption bands near the peak of the solar spectrum, high quantum conversion efficiencies, wavelengths suitable for using well developed optical materials, and they offer potentially fast cooling and recharging. As shown in figure 1, the absorption bands of the rhodamine 6G dye cover about 40 percent of solar spectrum in the wavelength region from 200 to 600nm. Especially the major absorption band centered at 530nm has 15 percent utilization of solar irradiance. The fluorescence quantum yield of the rhodamine 6G is reported in Ref. 1 to be about 95%.

In spite of these favorable characteristics of the rhodamine 6G, the threshold pump power to obtain lasing from it is still higher than that for the other solid and gas materials used for the solar-pumped lasers. The threshold pump-power density measured by Snively and Schafer [Ref. 2] with a flashlamp-pumping was  $4\text{kW/cm}^3$  for a  $5 \times 10^{-5}$  molar air saturated methanol solution of rhodamine 6G. The value obtained in our experiment was 20,000 solar constants and the corresponding absorbed power in the rhodamine 6G dye cell and the corresponding absorbed power in the rhodamine 6G dye cell was  $2\text{kW/cm}^3$ . The main factor causing the high threshold is the short lifetime of the upper laser level, which is of the order of 5-10ns, the overlap of the absorption and fluorescence spectra, and the triplet-triplet absorption. The reduction of the triplet-triplet absorption effect was achieved in our experiment by mixing the triplet quenching material COT with the dye solution. Dye laser amplifiers pumped by a flashlamp and by the Tamarack solar-simulator have been built and used to study the feasibility of solar-pumped dye lasers.

The spectral irradiances of the flashlamp and the Tamarack solar-simulator to provide various input powers, and the optimum dye concentration and oscillator's injection wavelength to obtain the high gain of the laser amplifier were also determined. Finally, the threshold pump-power was obtained by measuring the pump-power dependence of the amplifier gain.

## B. Experiment and results.

The experimental setups for the dye laser amplifier are shown in figures 2 and 3. In figure 2 the amplifier consists of a flashlamp and an rhodamine 6G dye cell which is cooled by the dye circulation, and oscillator used in this experiment was the tunable rhodamine 6G dye laser pumped by a  $N_2$ -laser (AVCO model C950) with a 60-percent transmitting output coupler, a 1200 groov/mm grating and a 1cm-long quartz dye cell. The output of the oscillator is split into two beams by using a beam splitter. One beam reflected from the front surface of the beam splitter goes to the monochromator, and then is detected by a photomultiplier tube. The other beam passing through the beam splitter is sent to the amplifier. The output from the amplifier is detected by an energy meter, a PM tube and an optical multichannel analyzer.

The first beam is used as a reference signal to normalize the amplifier output signal, and the difference of the normalized amplifier output with the pump-on from that with the pump-off becomes the gain of the amplifier. The gain measurements at high pump-power densities were made with the flashlamp because of the limited power densities available with the solar simulator. A pump-power range from 6,000 to 90,000 solar constants was obtained by varying the input energy of the flashlamp. The flashlamp used in this experiment was ILC-7L4.

The solar-simulator pumped dye laser amplifier is shown in figure 3. This setup is basically the same as that shown in figure 2 except the solar-simulator instead of the flashlamp is used for pumping. The solar-simulator beam is focussed by a cone-shaped collector to form a focal line on the axis where the dye cell is placed. The solar simulator used in this experiment was Tamarack xenon arc lamp, and its irradiance was adjusted to any number between 2,000 and 7,000 solar constants by varying the arc current. A 4-kW beam of 6,000 K blackbody spectrum similar to an air-mass-zero solar irradiance was obtained with this simulator. The calibration of the pump-power density was made by direct comparison with a tungsten-halogen standard source.

In Fig. 4 the spectral irradiance of the flashlamp at the maximum absorption peak wavelength of the Rhodamine 6G (530nm) as a function of the input energy is compared with that of the solar simulator at the same wavelength as a function of the arc current of the simulator. The spectral irradiance of the flashlamp at the electrical input energy 15 J is equal to 5,000 solar constants which is obtainable with the solar simulator at the arc current of 600A. A 4,300 solar constants from the solar simulator was used for the gain measurement of the laser amplifier at the low pumping power.

The injection time of the oscillator signal compared to the flashlamp-pump light is shown in Fig. 5. The oscillator was triggered with a time delay so that its laser output coincided with the peak time of the flashlamp signal. The flashlamp light pulse has 10- $\mu$ sec halfwidth and the risetime of 1.5 $\mu$ s.

Sample oscillograms of the input and output signals of the laser amplifiers are shown in Fig. 6. The gain measurements were made by recording a series of the output and input pulses on a dual-beam oscilloscope with the amplifier pump on and off. The output signals from the amplifier are nomalized

with respect to a uniform reference signal. Then, the apparent gain was determined by taking the difference of the output signal with the amplifier pump-on from that with pump-off. The observed FWHM of the signals were 70 ns.

Fig. 7 shows the apparent gain of the amplifier as a function of wavelength for  $1 \times 10^{-3}$  and  $7.5 \times 10^{-4}$  mole/liter solutions of rhodamine 6G in methanol. The dye cell used was 1-cm long and the pump intensity of the flashlamp was 36,000 solar constants. The error size of the data is about 2.1 percent at minimum. The maximum apparent gain was observed at the wavelength of 590nm, and the higher concentration gave higher apparent gains.

Fig. 8 shows the net gain of the 1 cm-long amplifier as a function of the rhodamine 6G concentration at the wavelength of 595nm. The net gain was determined by  $(S_2 - S_0)/S_0$ , where  $S_0$  is the output signal of the amplifier obtained with the methanol in the dye cell and  $S_2$  that with the dye solution (=Rh6G + methanol) in it. The amplifier-pumping power density used in these measurements was 36,000 solar constants. The maximum net gain was observed at  $1 \times 10^{-3}$  mole/liter, and this concentration was used for the gain measurement at different pump-power densities. For the concentrations higher than the optimum, absorption or negative gain was increased, and no net gain could be obtained.

Figure 9 shows the net gain of the amplifier as a function of amplifier pump power density at the 590nm wavelength. The dye cell used for the amplifier is a cuvette of 2-mm thick and 5 by 40-mm face area. The data obtained with the flashlamp are indicated by the black dots and that obtained with the solar simulator by a circled cross. The net gain increases linearly with the pump power from 2 to  $5 \times 10^4$  solar constants as expected from equation 9 in the appendix. The dotted line, which was obtained by taking account of the absorption through the unpumped length in the cell, shows that a pump power larger than 20,000 solar constants (or  $2.7 \text{ kW/cm}^2$ ) is required at the dye

cuvette to obtain the positive net gain. This value corresponds to a pump power density of

$$2.7 \text{ kW/cm}^2 \times (0.5 \times 4.0 \text{ cm}^2) / (0.2 \times 0.5 \times 4.0 \text{ cm}^3) = 13.5 \text{ kW/cm}^3,$$

and an absorbed pump power density of  $2.0 \text{ kW/cm}^3$  ( $= 13.5 \text{ kW/cm}^3 \times 0.15$ ) in the dye. The result obtained with the solar simulator is in agreement with the extrapolation of the flashlamp results. In spite of the slow risetime of the solar simulator pulse which is about 1 ms, the solar simulator output chopped to 4-ms pulses was used in this measurement, while the flashlamp pulse had about 10-microsecond halfwidth. The population of the dye molecule in the triplet states might be built up during the slow rise time of the chopped-pump pulse. The presence of the triplet quencher (COT) may help alleviating the reduction of the gain. Only 4,300 solar constants, at best, were obtained with the present experimental setup.

### C. Summary and conclusion

- (i) Flashlamp and solar-simulator (Tamarack) irradiance measurements were made.
- (ii) Threshold pump power was determined to be approximately 20,000 solar constants or  $2 \text{ kW/cm}^3$  for the 590nm tuned injection into the  $1 \times 10^{-3}$  mol/liter rhodamine 6G dye cell.
- (iii) The threshold measured is one half of that reported by Snavely and Schafer (1969).

This study indicates that with an improved beam collecting method, it is feasible to realize the solar-pumped dye laser. A new collecting system of the solar-simulator beam is currently under development.



#### D. List of Figures

- Figure 1. The comparison of the absorption and emission spectra of rhodamine 6G with the air-mass-zero solar spectrum.
- Figure 2. Schematic diagram for the experimental setup with a flashlamp pumping.
- Figure 3. Schematic diagram for the experimental setup with the Tamarack solar-simulator pumping.
- Figure 4. Spectral irradiance of flashlamp and solar simulator.
- Figure 5. Injection time of the oscillator beam relative to the flashlamp signal.
- Figure 6. Representative oscilloscope displays of the input and output signals of the amplifier cell.
- Figure 7. Apparent gain as a function of wavelength for  $1 \times 10^{-3}$  molar and  $7.5 \times 10^{-4}$  molar solutions of rhodamine 6G in methanol.
- Figure 8. Net gain of a 1 cm-long amplifier as a function of the rhodamine 6G concentration at the wavelength of 595 nm.
- Figure 9. The net gain of the rhodamine 6G dye-laser amplifier as a function of amplifier pump power density at the 590nm wavelength.

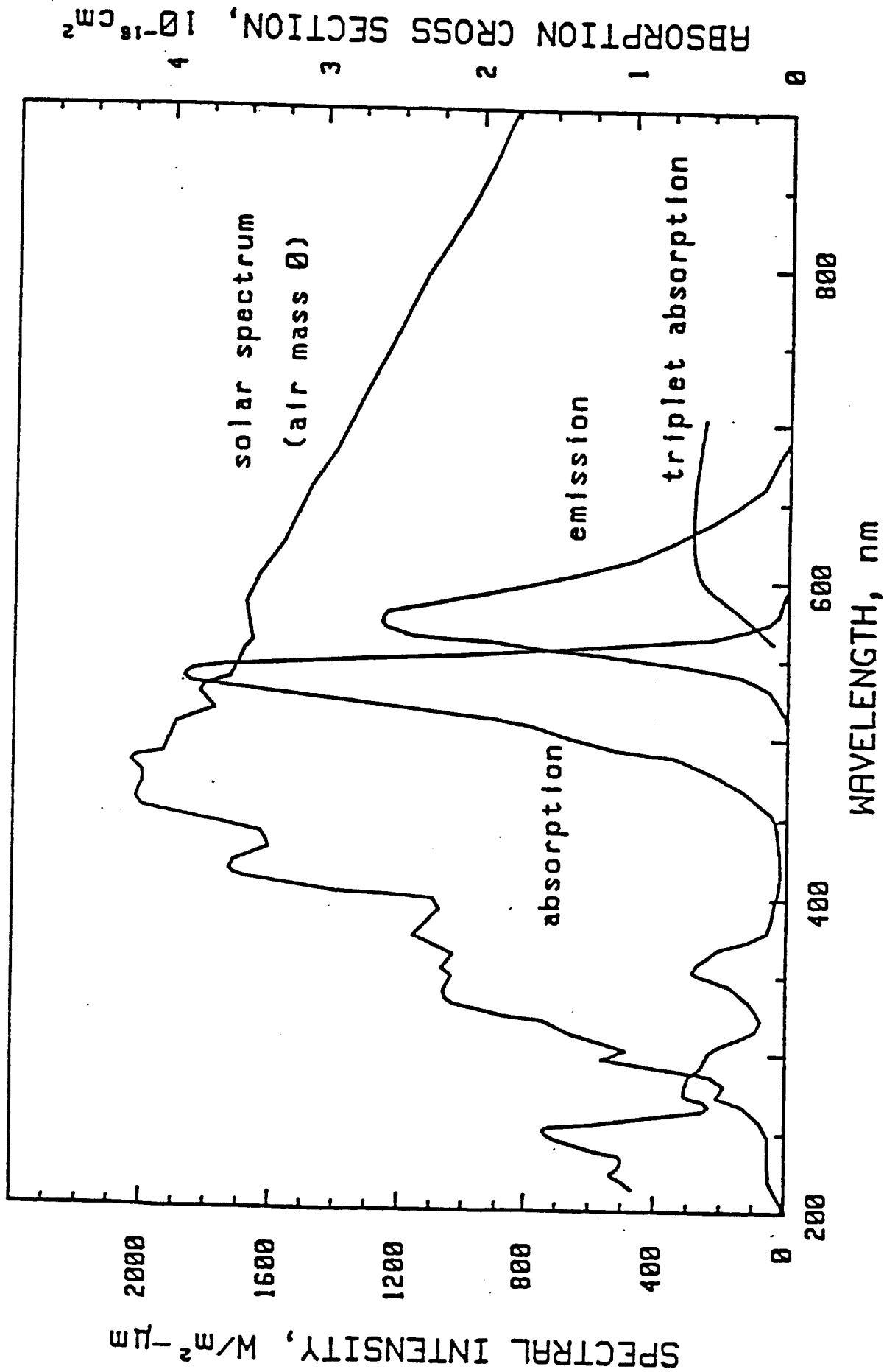


Figure 1. The comparison of the absorption and emission spectra of rhodamine 6G with the air-mass-zero solar spectrum.

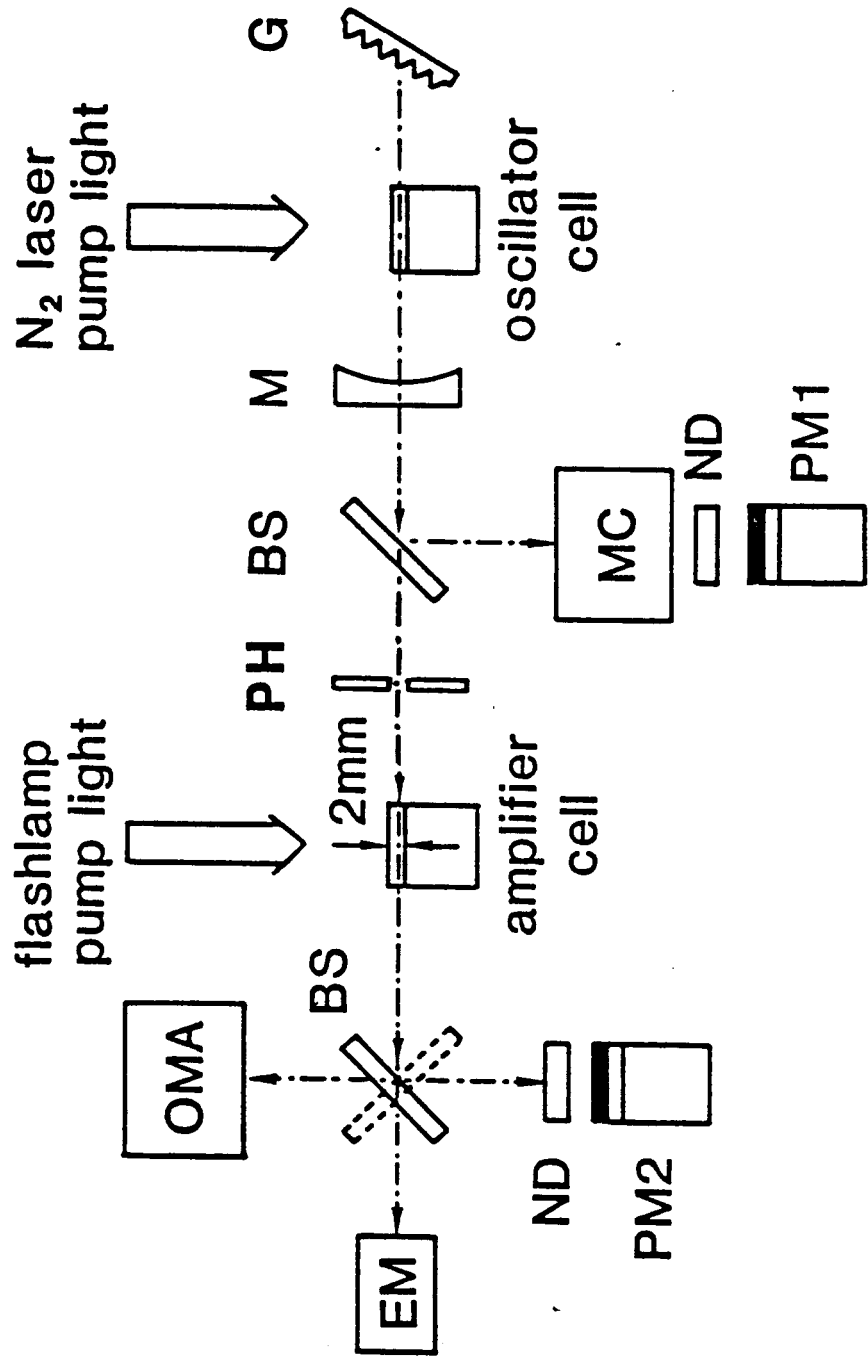


Figure 2. Schematic diagram for the experimental setup with a flashlamp pumping.

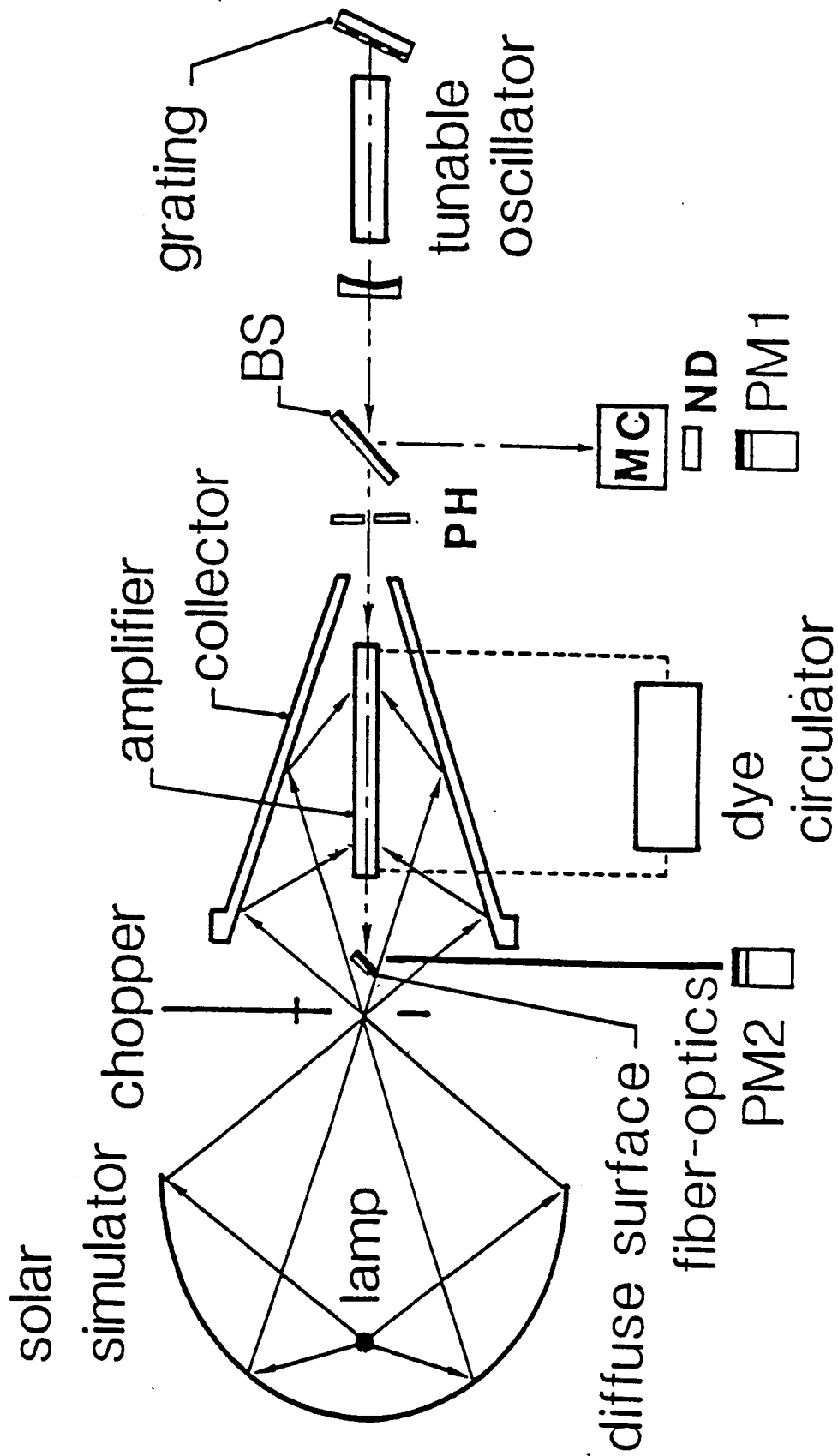


Figure 3. Schematic diagram for the experimental setup with the Tamarack solar-simulator pumping.

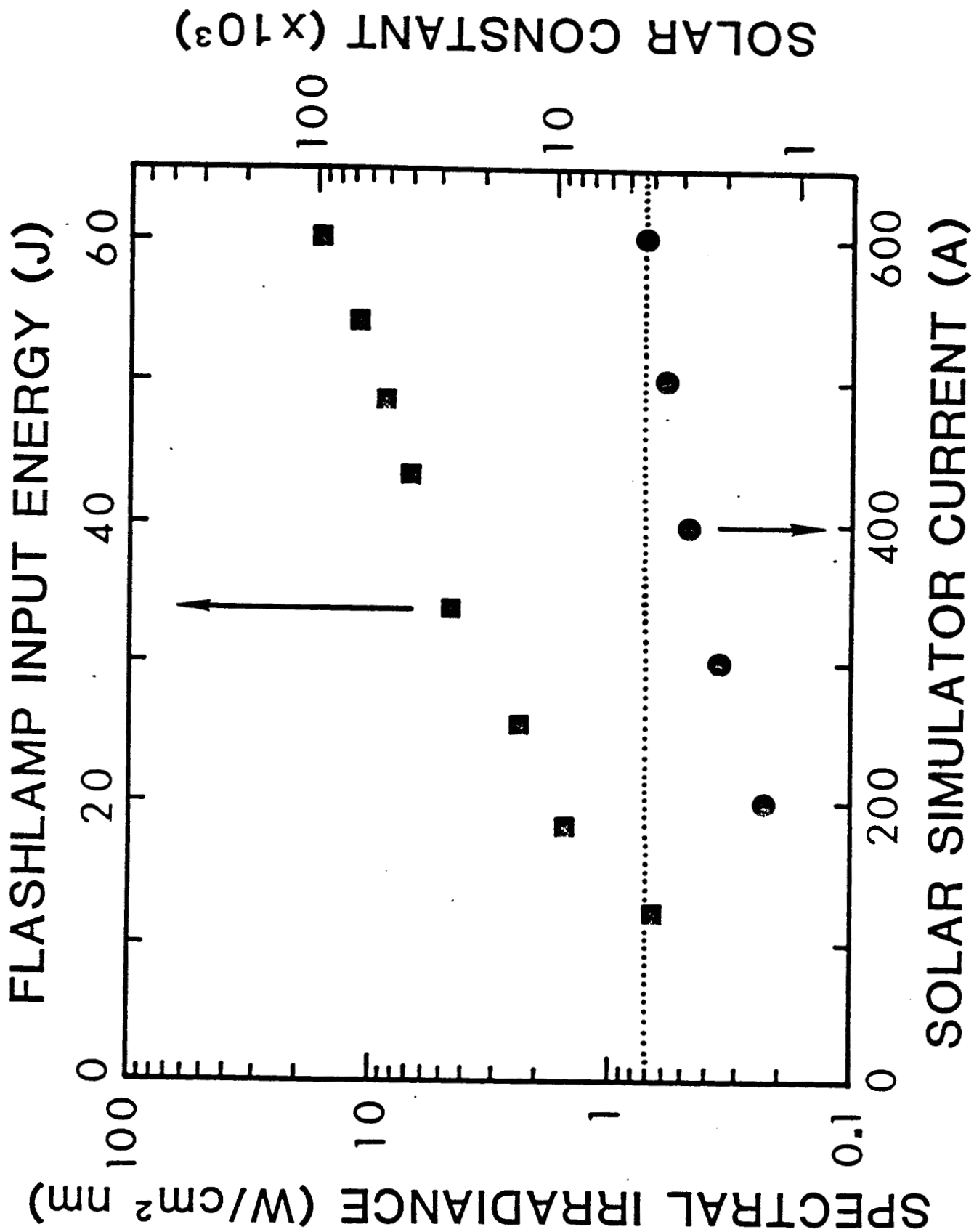
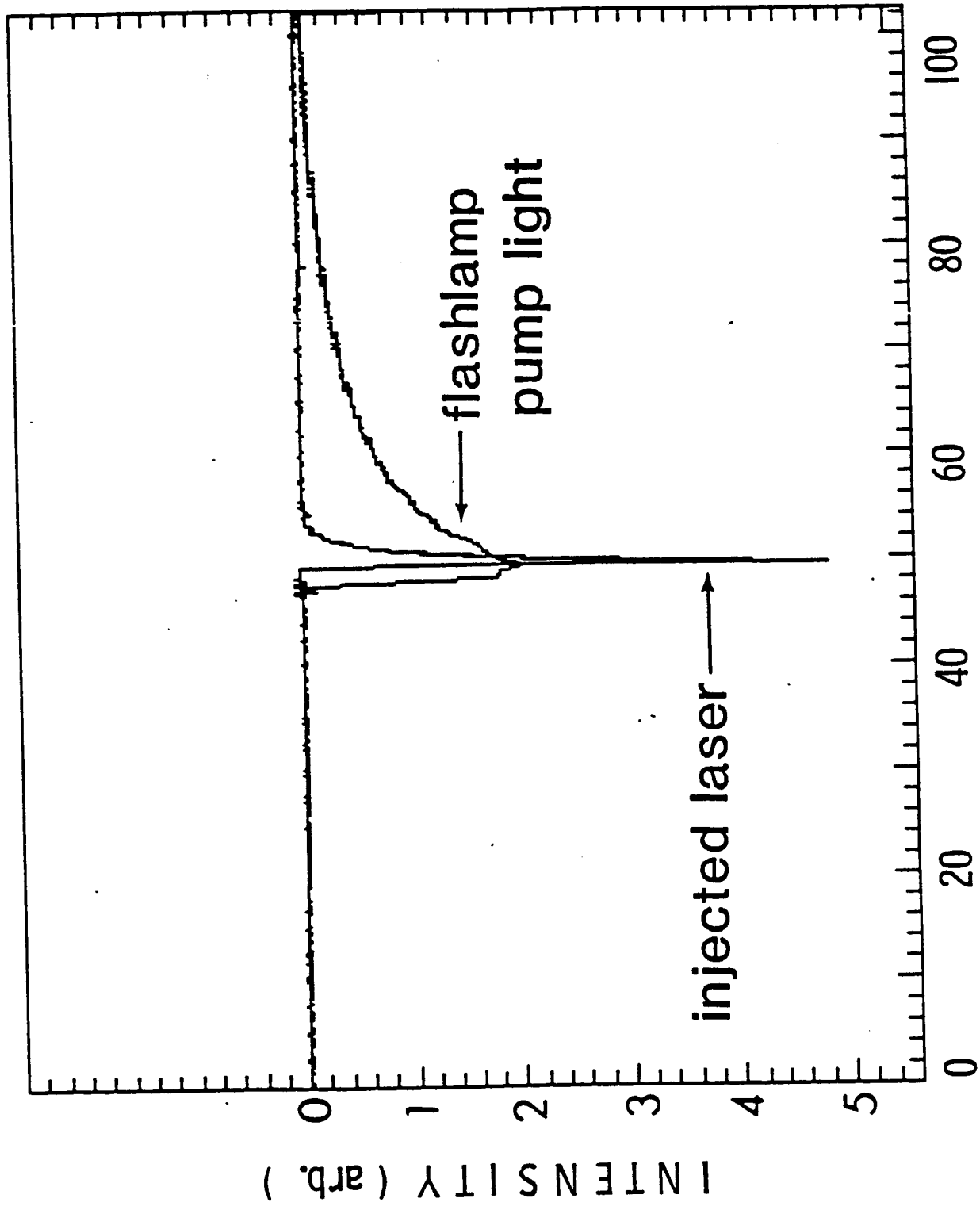


Figure 4. Spectral irradiance of flashlamp and solar simulator.



TIME (microsec. )

Figure 5. Injection time of the oscillator beam relative to the flashlamp signal.

ORIGINAL PAGE IS  
OF POOR QUALITY

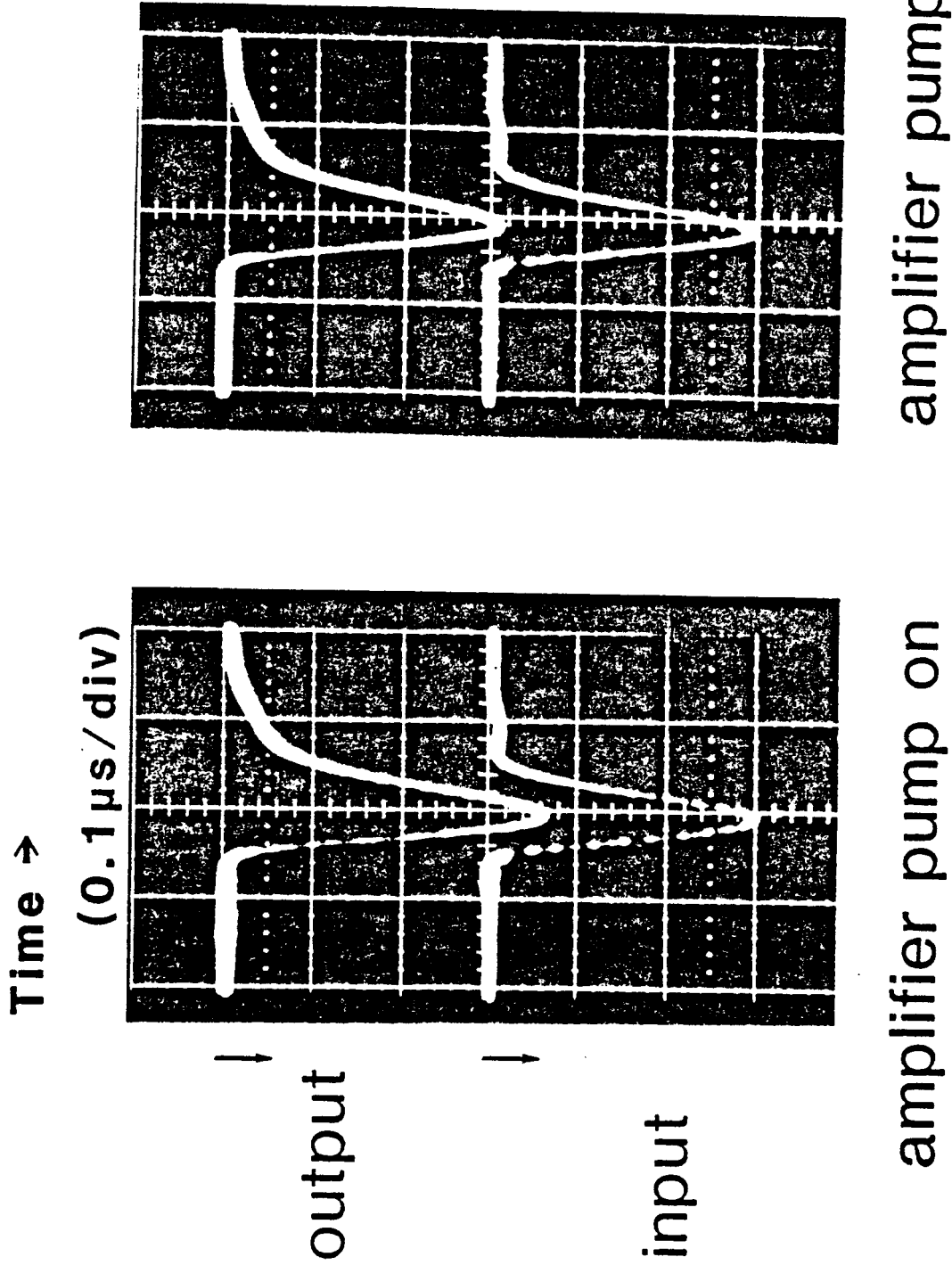


Figure 6. Representative oscilloscope displays of the input and output signals of the amplifier cell.

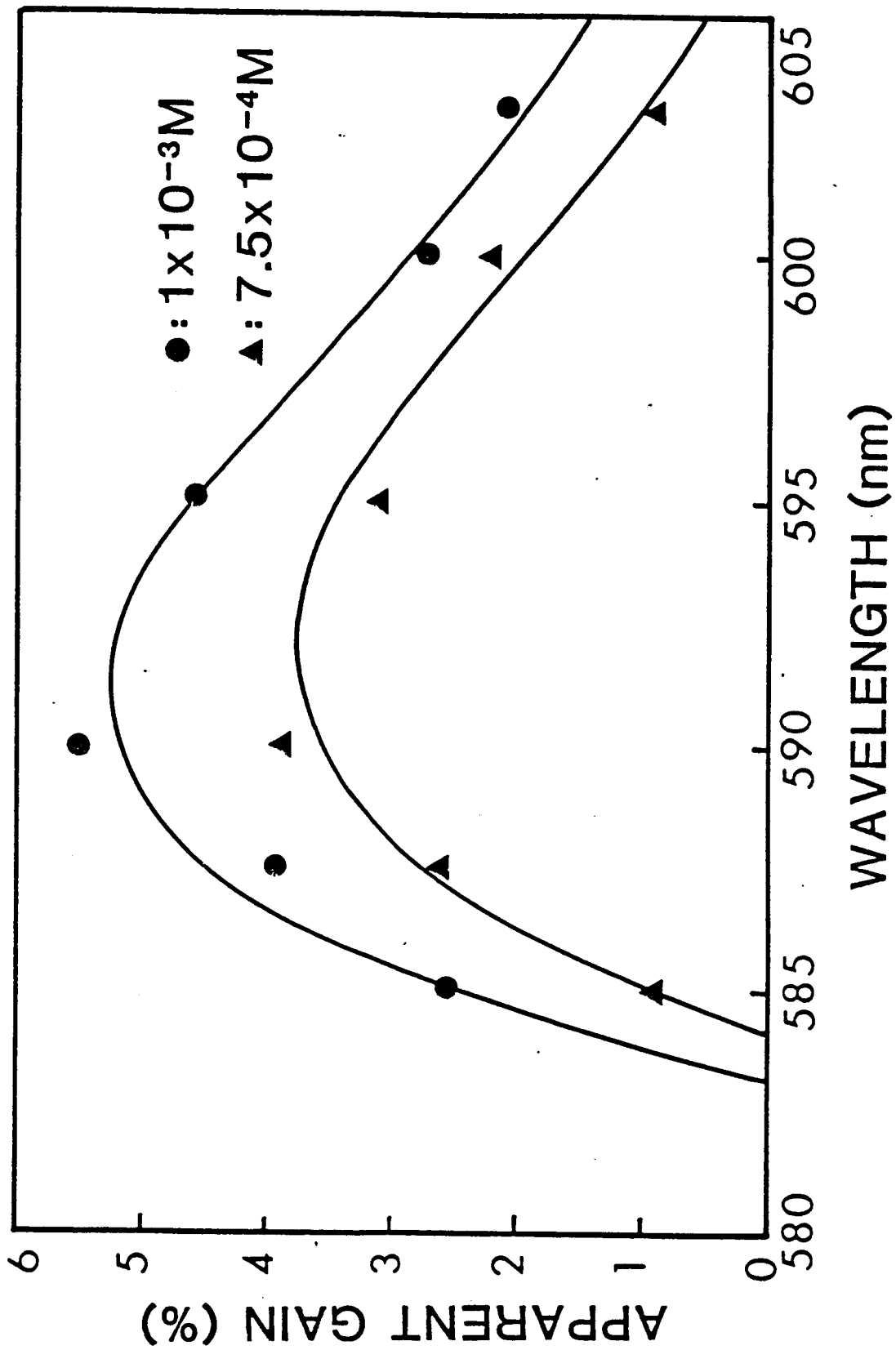


Figure 7. Apparent gain as a function of wavelength for  $1 \times 10^{-3} \text{M}$  and  $7.5 \times 10^{-4} \text{M}$  solutions of rhodamine 6G in methanol.



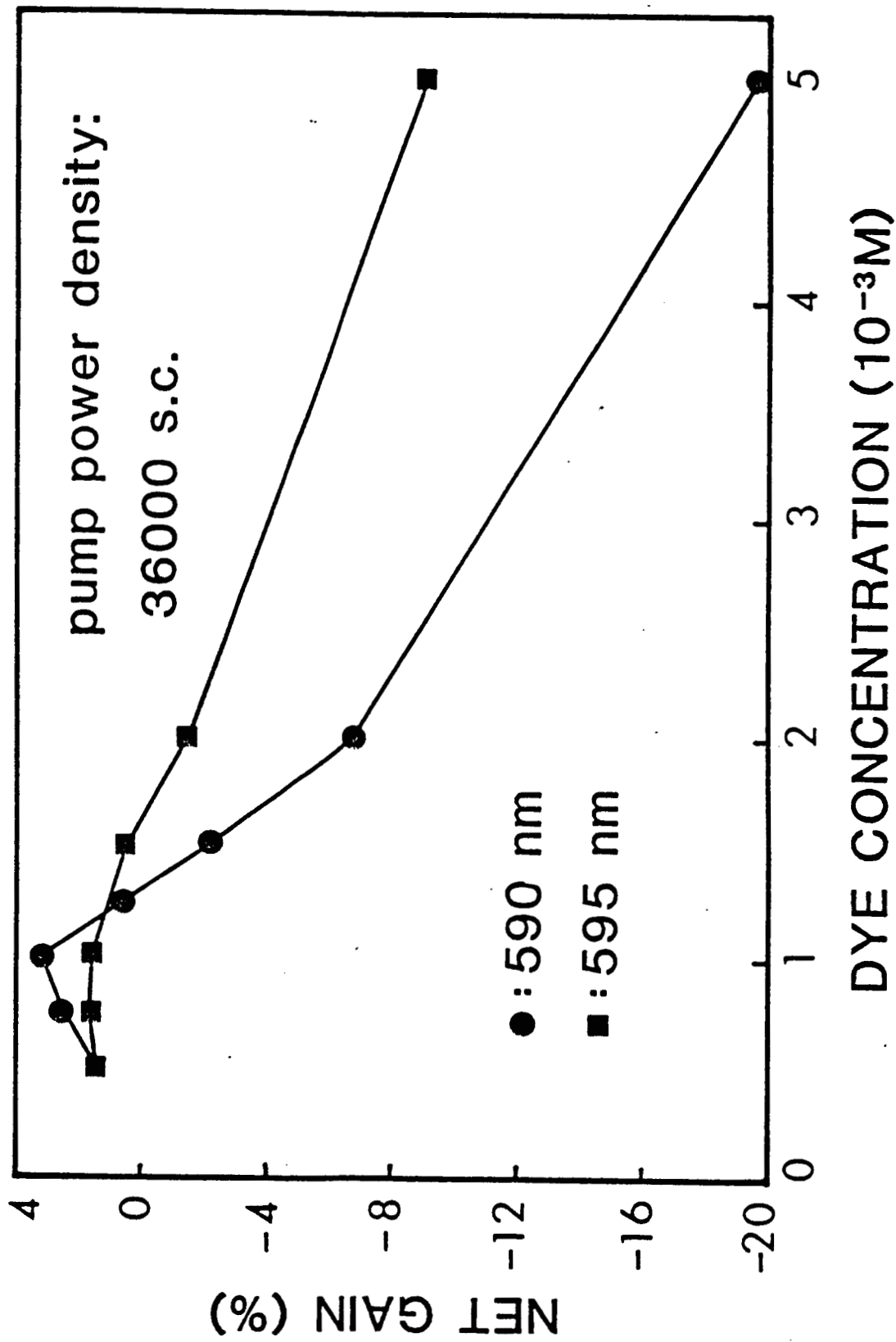


Figure 8. Net gain of a 1 cm-long amplifier as a function of the rhodamine 6G concentration at the wavelength of 595 nm.

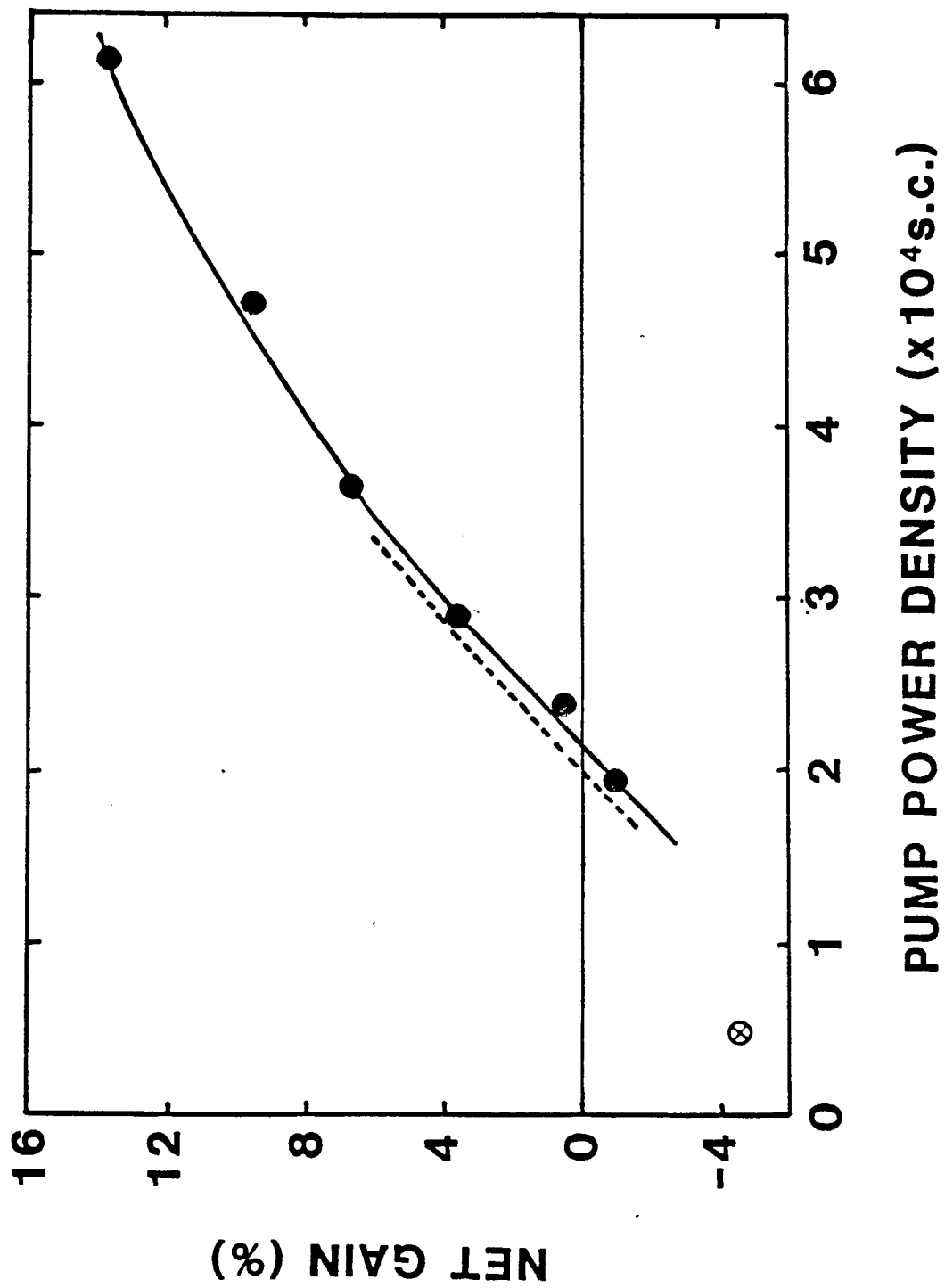


Figure 9. The net gain of the rhodamine 6G dye-laser amplifier as a function of amplifier pump power density at the 590nm wavelength.

# DYE LASER GAIN

## 1. Single Pass Gain

$$G = \exp(gl) \quad (1)$$

where  $g = N_1 B/c - N_0 \epsilon_{ss} - N_T \epsilon_{TT}$  : Gain coeff. (2)

$$B = \frac{\lambda^4 E(\lambda) \eta}{8 \pi \tau} \quad (3)$$

$l =$  gain length

[Ref. 3]

Rate equations for the dye laser

$$\frac{dN_1}{dt} = N_0 W - N_1/\tau - BqN_1 \quad (4)$$

$$\frac{dN_T}{dt} = N_1 k_{ST} - N_T/\tau_T \quad (5)$$

$$N = N_0 + N_1 + N_T \quad (6)$$

For the steady state ( $\frac{dN_i}{dt} = 0$ ), small signal input ( $Bq \ll 1$ ), and weak pump intensity ( $W \ll 1$ )

$$N_1 = NWT \quad (7)$$

$$g = N[W_T(B/c + \epsilon_{SS}(1+k_{ST}T)) - \epsilon_{TT}k_{ST}T] - \epsilon_{SS} \quad (8)$$

With the triplet quencher & fast flow of dye solution

$$\epsilon_{TT} \approx 0$$

$$k_{ST}T \ll 1$$

$$\approx N[W_T(B/c + \epsilon_{SS}) - \epsilon_{SS}]$$

If  $g \ll 1$ ,

$$G = \exp(g) \approx 1 + g$$

$$= 1 + [NW_T(B/c + \epsilon_{SS}) - \epsilon_{SS}N] \quad (9)$$

2. Threshold

$$G = 1 \rightarrow g = 0 \quad \text{:Threshold}$$

$$0 \leq \underbrace{NW_T(B/c + \epsilon_{SS}) - \epsilon_{SS}N}_{\text{Apparent gain}} \quad \text{:Net gain}$$

Reabsorption

## F. References

1. F. P. Schafer "Dye Lasers" Springer-Verlag, New York (1977).
2. B. B. Snavely and F. P. Schafer "Feasibility of CW operation of dye lasers" Phys. Lett. 28A (11), 728 (1969).
3. B. B. Snavely "Flashlamp-Excited Organic Dye Lasers" Proc. IEEE., 57 (8) 1374 (1969).

## II. Kinetic Modeling of Solar-Pumped Iodine Laser

### A. Introduction and Results

This report relates the work performed during the period of April 1, 1986 through Sept 30, 1986. During this period, the work to construct a kinetic model algorithm which predicts the output parameters of a laser (lasing time, time to threshold, and pulse energy) has progressed. To this date the kinetic model has improved such that there is good agreement between the theoretical model and the experimental data for the systems defined in the previous progress reports as flashlamp-pumped iodine laser oscillator system (which was characterized by a cylindrical resonator cavity and pumping times of about one millisecond), and the long path-length solar-pumped laser (rectangular resonator cavity and pumping times of about one second). Both experimental data sets are for the lasing gas  $\text{i-C}_3\text{F}_7\text{I}$  whose kinetic reaction rates are well known if compared with other iodide. Once the results of the fit for this relatively well known gas for the two systems are qualified, other gases and their subsequent kinetic rates can be studied with greater confidence. In table I their reactions and reaction rates are given with experimentally found bounds. Subsequently, the reaction rates given in table II are within the experimental bounds and are used to fit the data for the two experiments mentioned above. The box laser's results are preliminary and the differences between two systems have yet to be resolved.

Using the kinetic equations as given in NASA TP 2241 except that the diffusion time is assumed to be infinite, a set of reaction rates is found (Table II) for the rectangular resonator cavity. These rates are found using a data set (Table III) which the pumping light intensity and the output mirror

reflectivity are varied. Using numerical methods, a much higher cavity loss is found for the optical path (52%). These losses are introduced into the model as mirror losses and agree with the total cavity losses reported by Dr. DeYoung's article in the IEEE Journal of Quantum Electronics, Vol. QE-22, No. 7, July 1986 for the same experiment. Comparing the lasing time experimental data and the theoretical results (Table III) for the 85% output mirror, the lasing time for the theory is decreasing for a less intense pumping source. On the other hand, the experimental data dictates an increasing lasing time as the pumping power decreases. This indicates that there is a mechanism which increases the gain relative to the light input as the system lases; diffusion may solve these problem. Upon introducing the added loss to the system and after fitting the data, the result is given in figure 1. The theory now better predicts the experimental data. At high pressure the lasing times are approximately the same for the two mirrors, and the threshold times and the pulse energies are proportional for the two different mirrors. The problem still remains that the experimental data for the pulse energies is given for total energy output (Joules), and the calculation is for the energy output at the center line (Joules/cm<sup>2</sup>).

By introducing the heat equation, the diffusion time constant, the light input, and the photodissociation cross sections as reported by the previous progress report into the kinetic model given by NAS TP2241, the kinetic model is modified to incorporate a cylindrical laser cavity. The experimental data is given in the table IV for the flashlamp-pumped iodine (i-C<sub>3</sub>F<sub>7</sub>I) oscillator system, and is closely approximated by the theoretical predictions for the lasing time, time to lasing threshold, and pulse energy output (figure 2, 3 and 4). The theoretical model uses a test pulse for the uv light input and includes a 9% optical path which was found experimentally. The actual light

input varies as much as ten percent; this explains much of the deviation from the data by theory.

A further modification was made by the introduction of an initial  $[I_2]$  as a function of pressure, given by

$$[I_2] = (1/9) \times 10^{(14.878 - 0.09522P)} + 2.92 \times 10^{11} P + 1.45 \times 10^{11} P^2 + 2.7164 \times 10^{14},$$

where  $P$  is the fill pressure. The introduction of  $[I_2]$  best describes the quenching detected at threshold and at the end of the laser pulse. When the figures of the gas densities as a function of lasing time (figure 5, 6, 7 and 8) are examined,  $[I_2]$  is initially high, and as the system lases  $[I_2]$  density increases until lasing is terminated. The theoretical prediction for the power agrees very well with the data given for the power output of the laser (figures 9, 10, 11, and 12) for different pressures.

In figure 13 the non-quasi-steady-state solution is shown and compared to the quasi-steady-state approximation (solid line). The theoretical model also agrees with the relaxations in the power output as a function of time given by the digital oscilloscope. Furthermore, the theoretical output parameters shown in figures 2, 3, and 4 are compared for the two different solutions. It can be seen that they agree, therefore, the quasi-steady-state solution can be used for the theoretical predictions of the output parameters of different laser configurations.

The refinement of the kinetic model and the subsequent ability to analyze a laser system are further improvement of the technique to optimize a solar-pumped space-based laser power station. By attempting to fit the data other mechanisms in addition to the kinetics which may fundamentally alter the output parameters of the laser system are identified.



## List of figures

- Figure 1 - A comparison of the output parameters of the rectangular laser cavity for two different output mirror reflectivities.
- Figure 2, 3 and 4 - A comparison of the output parameters for the laser with a cylindrical cavity. Its experimental data and two theoretical predictions, quasi-steady-state solution and nonquasi-steady-state solutions.
- Figure 5, 6, 7 and 8 - Theoretical predictions of gas and photon densities normalized to their peak value along with an experimental data sampling (squares) of the photon density coming out of the laser for different pressures.
- Figure 9 - The quasi-steady-state approximation compared to the theoretical prediction (dotted line) for the power output of the laser as a function of time. The peak power of the quasi-steady-state solution is used to normalize the theoretical prediction of the power output. The flashlamp pulse power experimental data is given as is the laser output power data.
- Figure 10, 11, 12, and 13 - The experimental flashlamp pulse power data and the laser output power data compared to the theoretical power output data for different pressures.

ORIGINAL PAGE IS  
OF POOR QUALITY

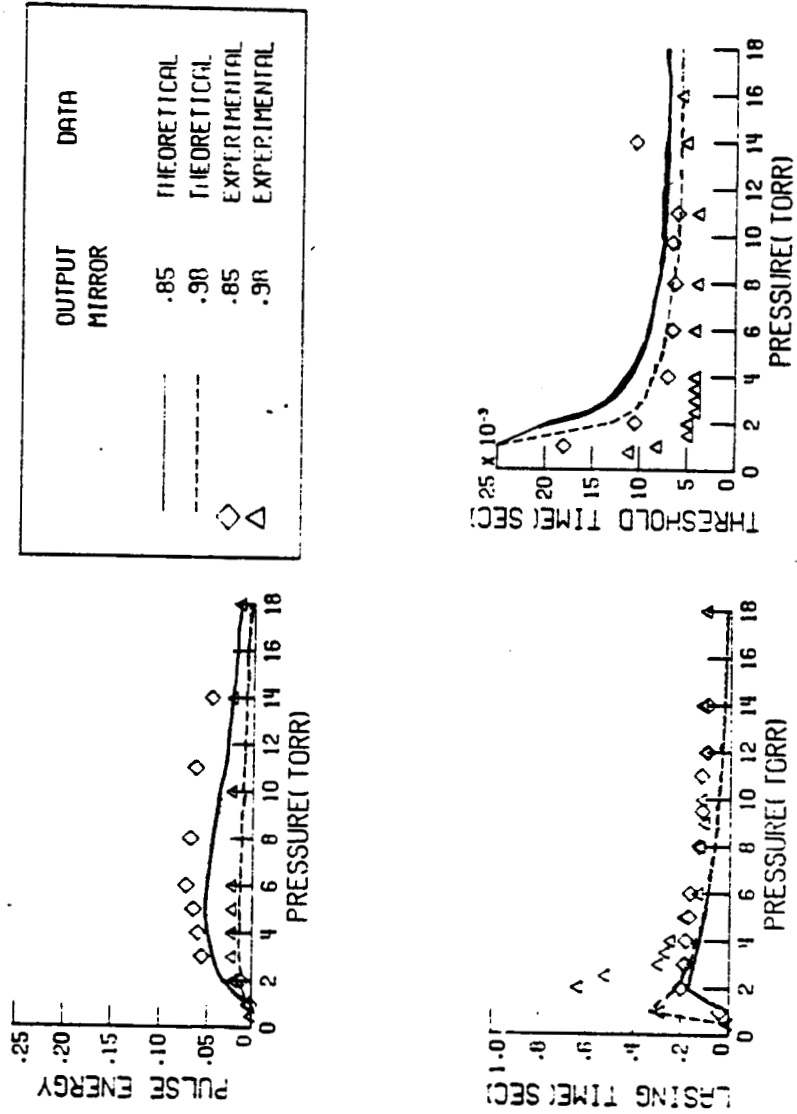


Figure 1

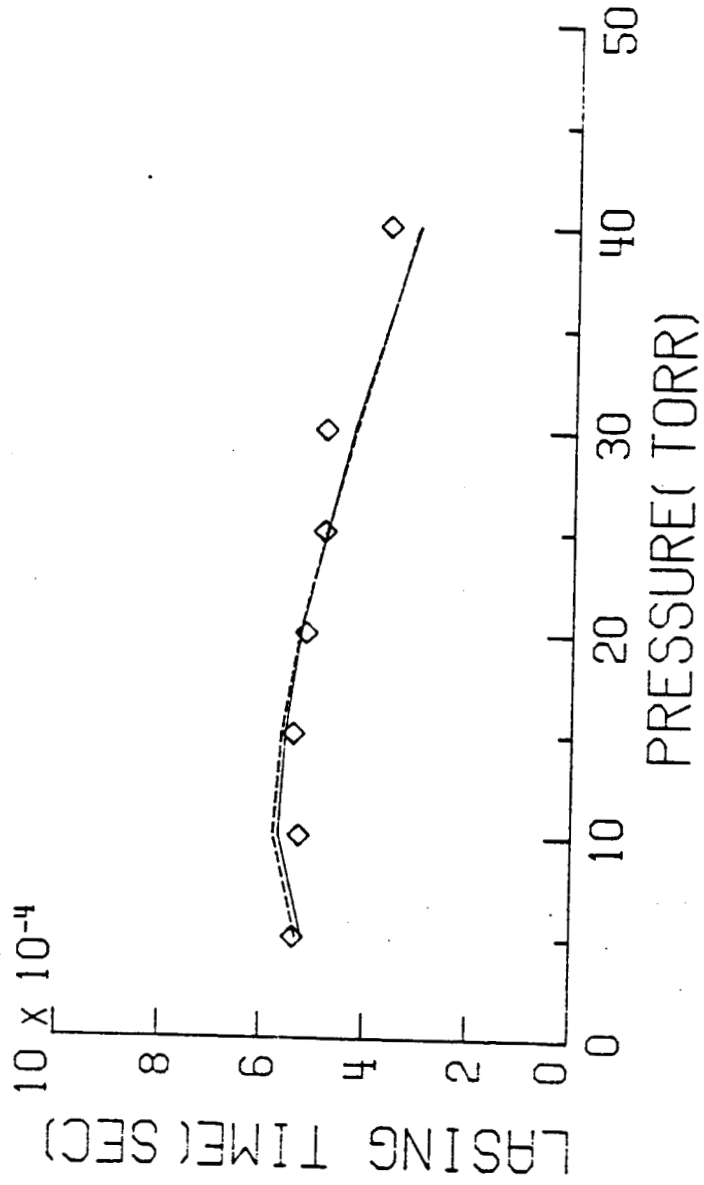
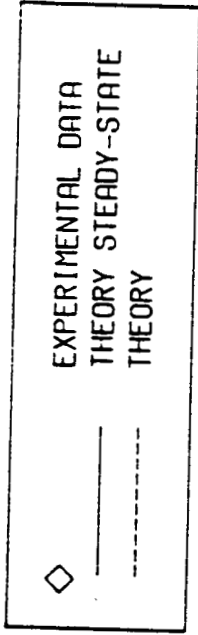


Figure 2

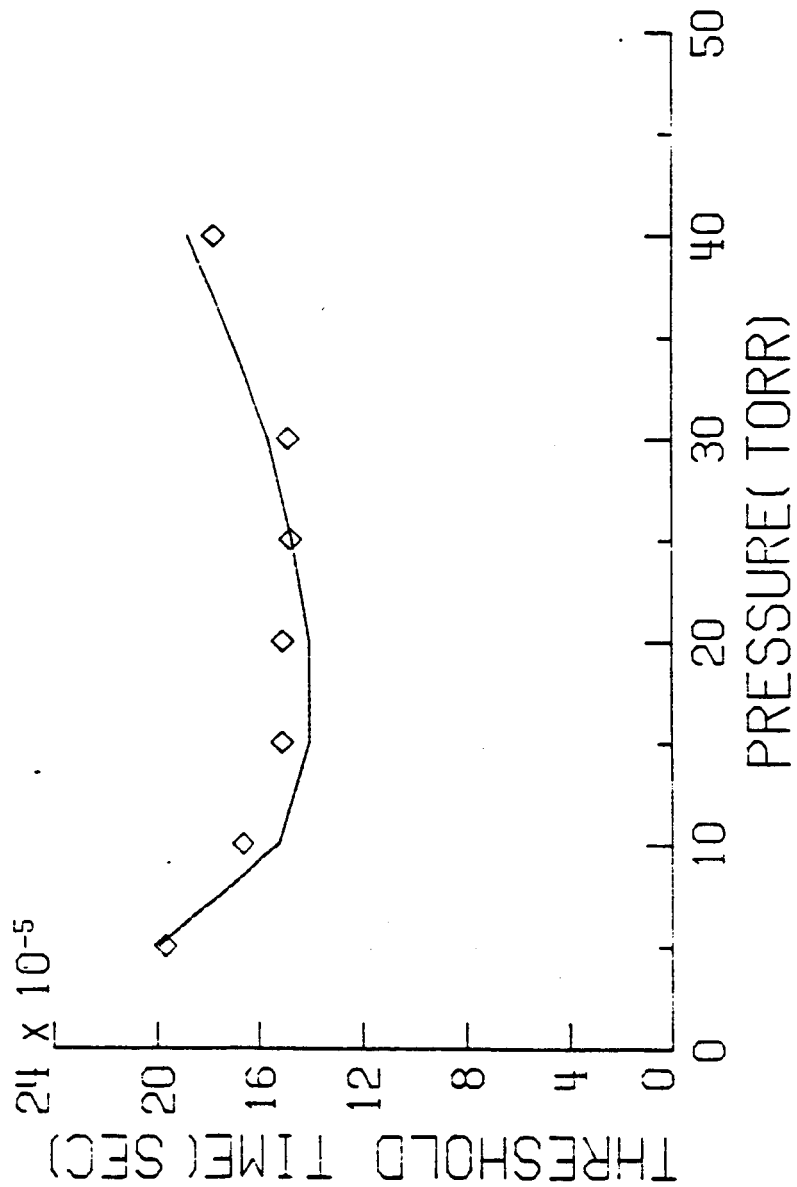
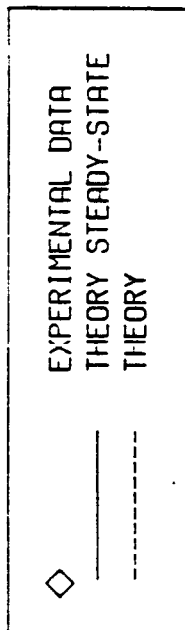


Figure 3

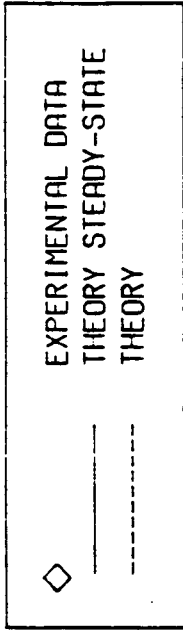
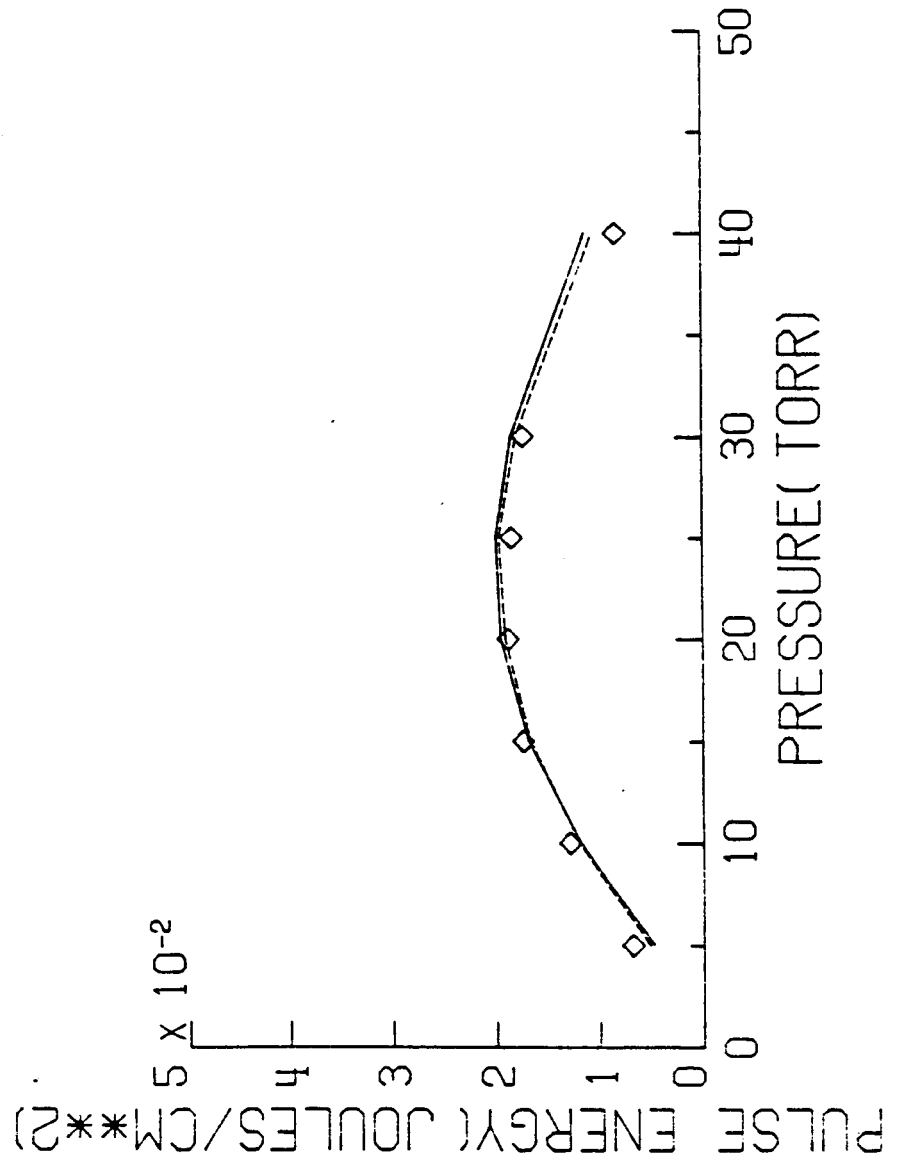


Figure 4

5 TORR

DENSITY	PEAK VALUE
1S1	.191E+16
R2	.194E+16
I	.175E+16
12	.342E+15
R	.101E+16
RHO	.475E-07

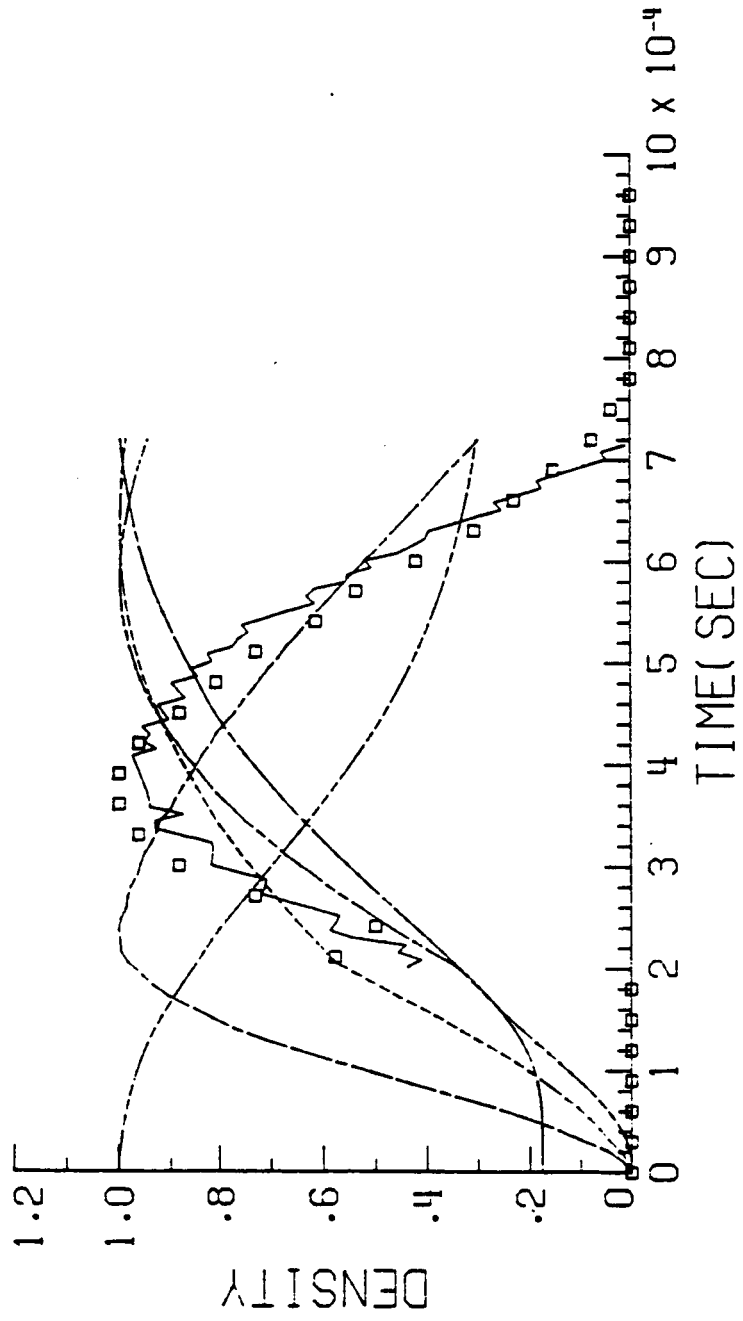


Figure 5

15 TORR

DENSITY	PEAK VALUE
---	.362E+16
---	.389E+16
---	.400E+16
---	.424E+15
---	.148E+16
---	.159E-06

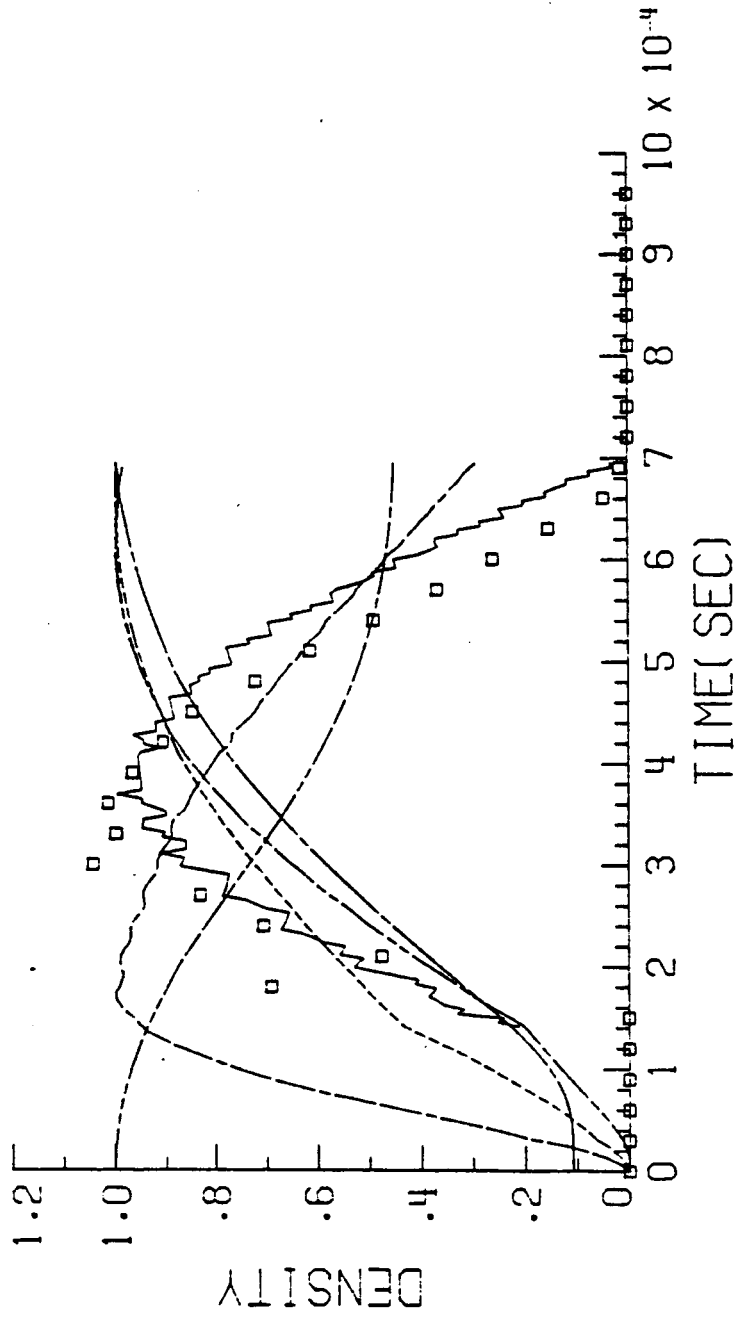


Figure 6

DENSITY	PEAK VALUE
1ST	.554E+16
R2	.600E+16
I	.627E+16
I2	.637E+15
R	.191E+16
RHD	.225E-06

30 TORR

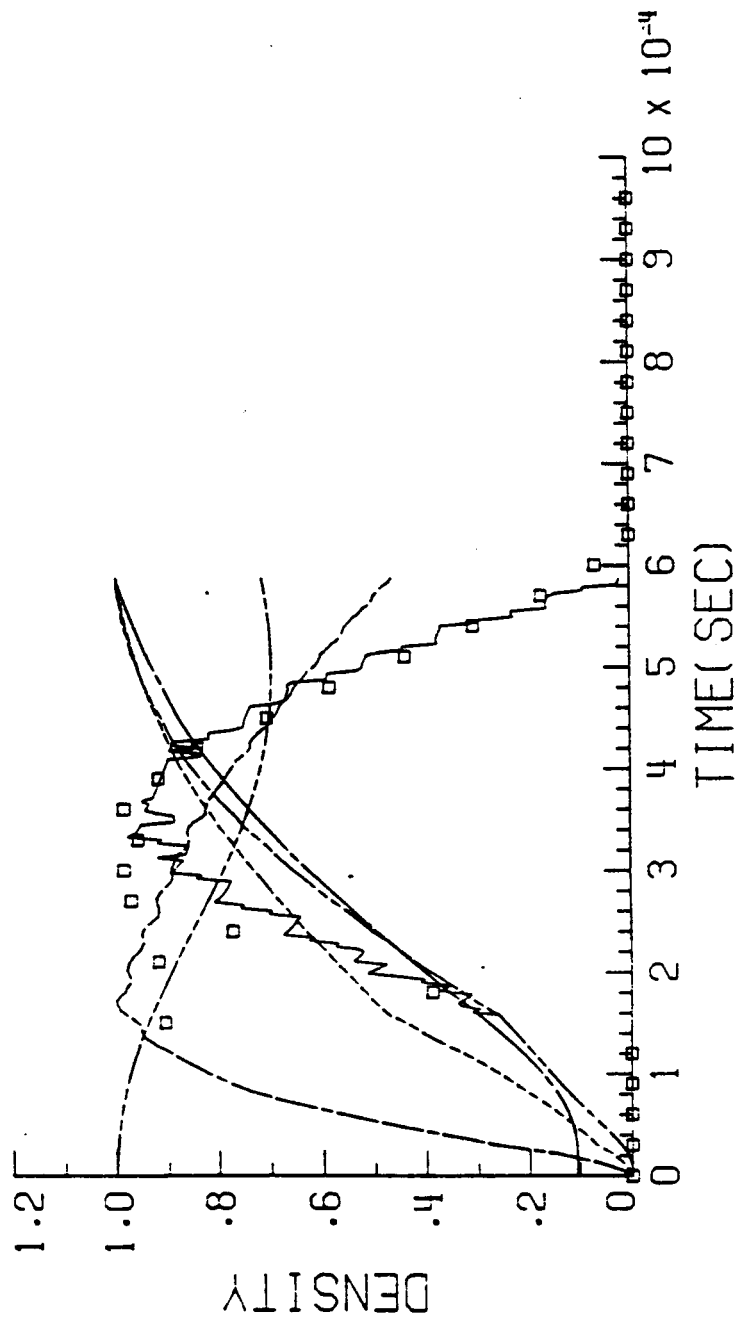


Figure 7



40 TORR

DENSITY	PEAK VALUE
---	.635E+16
---	.679E+16
---	.710E+16
---	.816E+15
---	.208E+16
---	.191E-06

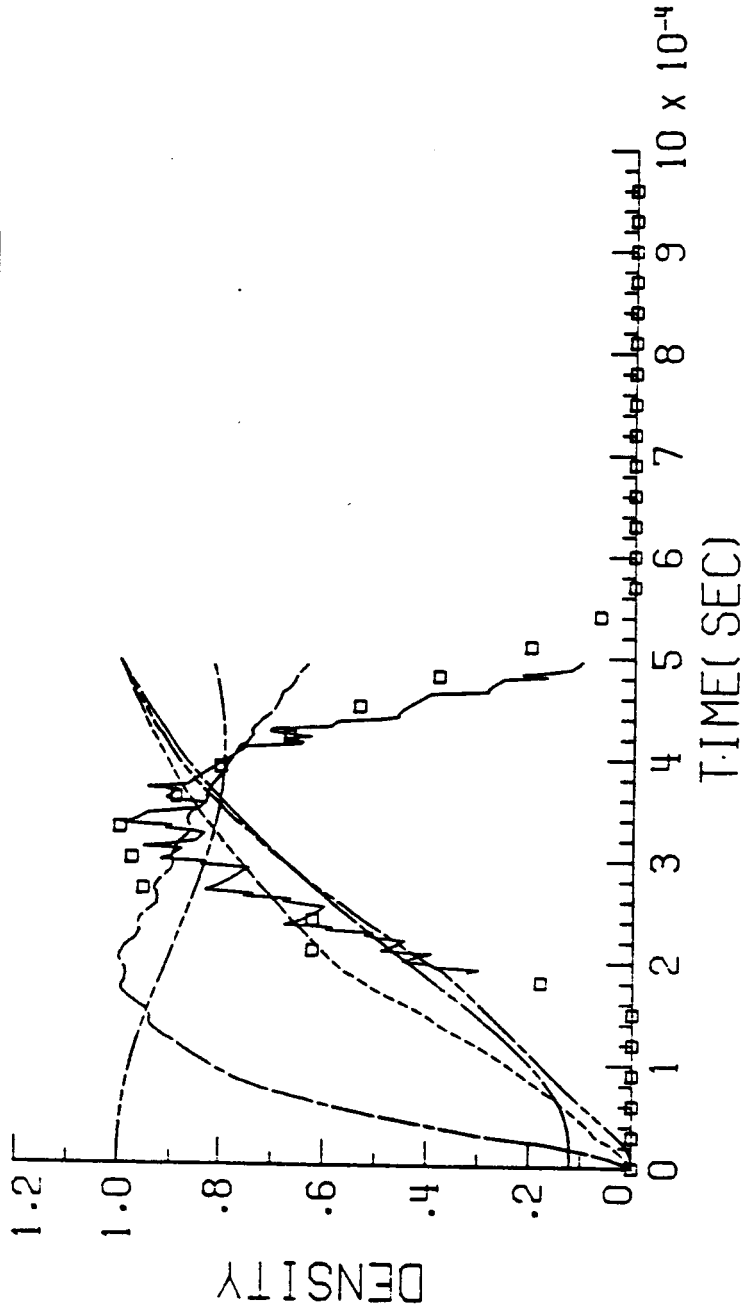


Figure 8

5 TORR

ALL PULSES NORMALIZED  
TO THEIR PEAK VALUE

— QJMSJ-STEADY STATE  
PULSE POWER DATA

· LASER POWER DATA

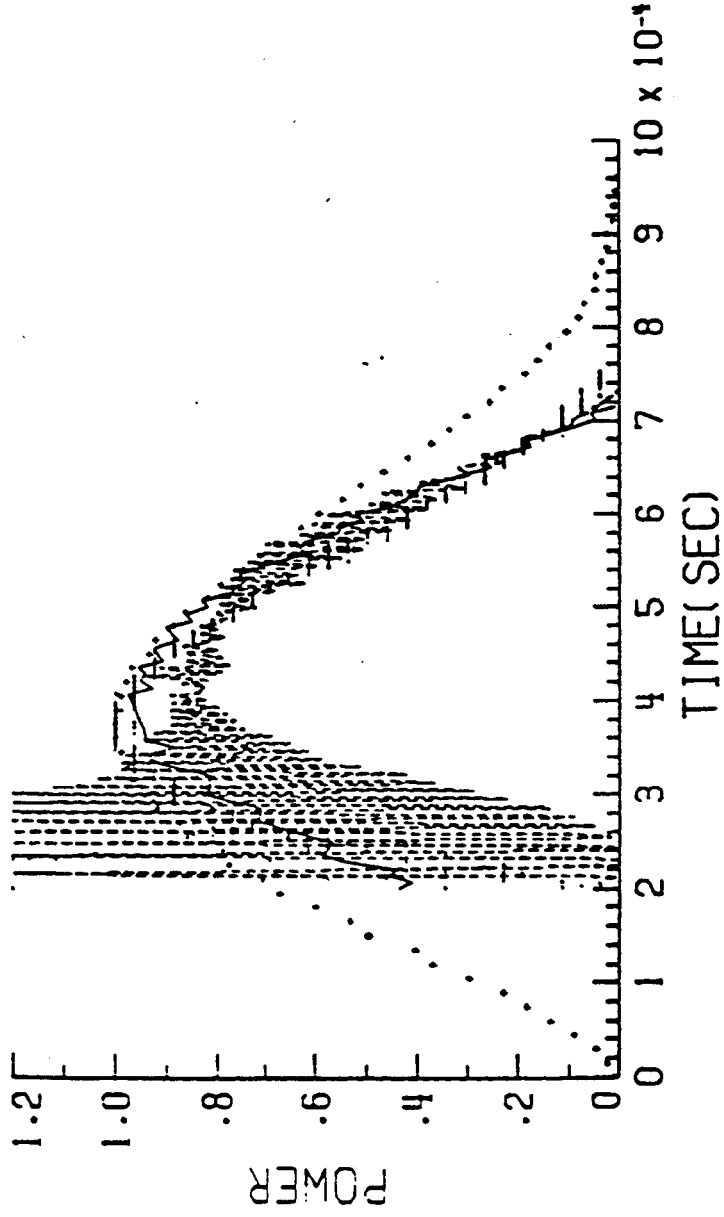


Figure 9

5 TORR

ALL PULSES NORMALIZED  
TO THEIR PEAK VALUE

— QUASI-STEADY STATE  
PULSE POWER DATA

+ · LASER POWER DATA

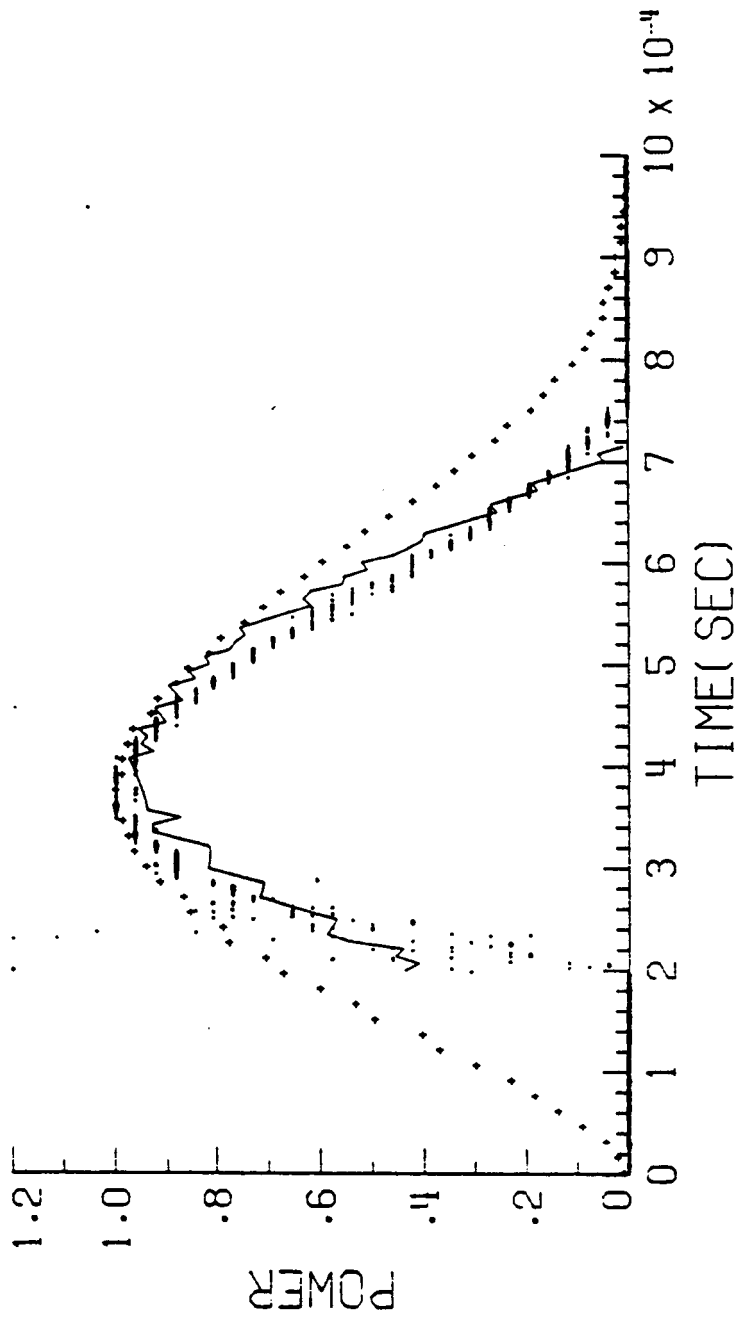


Figure 10

15 TORR

ALL PULSES NORMALIZED  
TO THEIR PEAK VALUE

— QUASI-STEADY STATE  
PULSE POWER DATA  
+ LASER POWER DATA

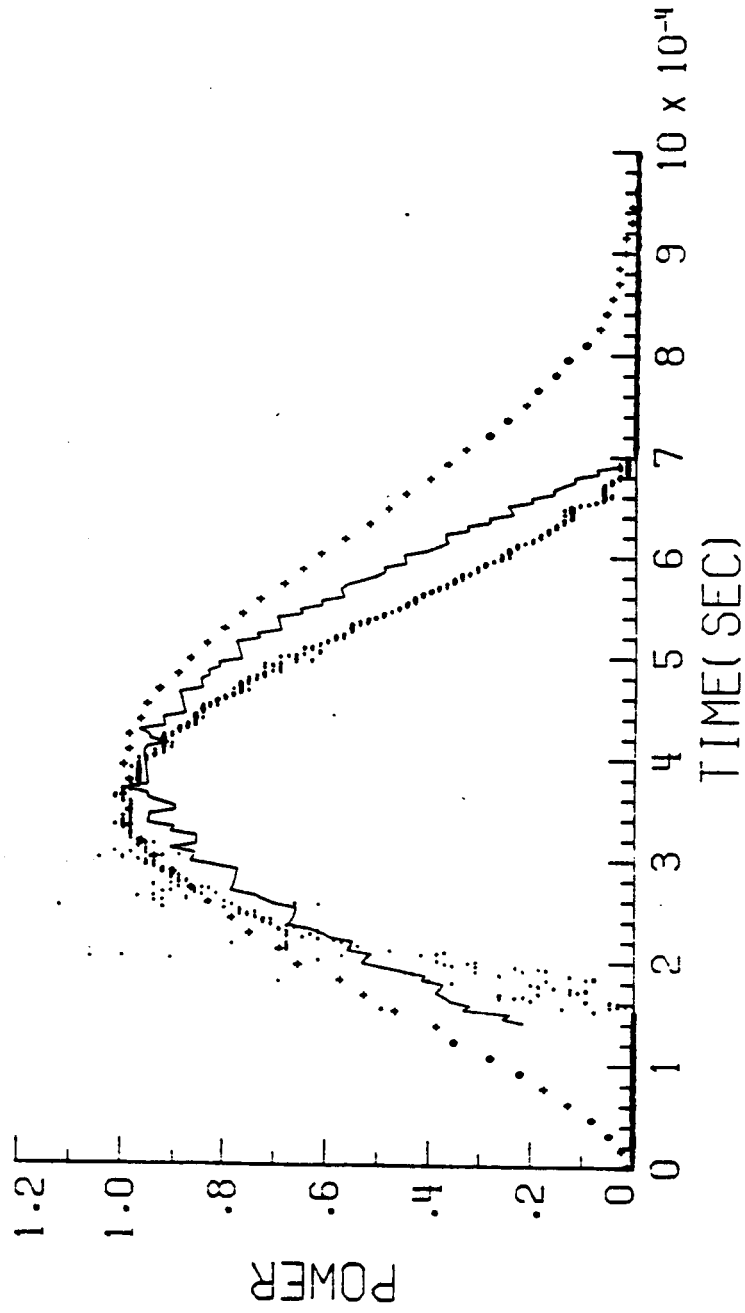


Figure 11

30 TORR

ALL PULSES NORMALIZED  
TO THEIR PEAK VALUE

— QUASI-STEADY STATE  
PULSE POWER DATA

+ LASER POWER DATA

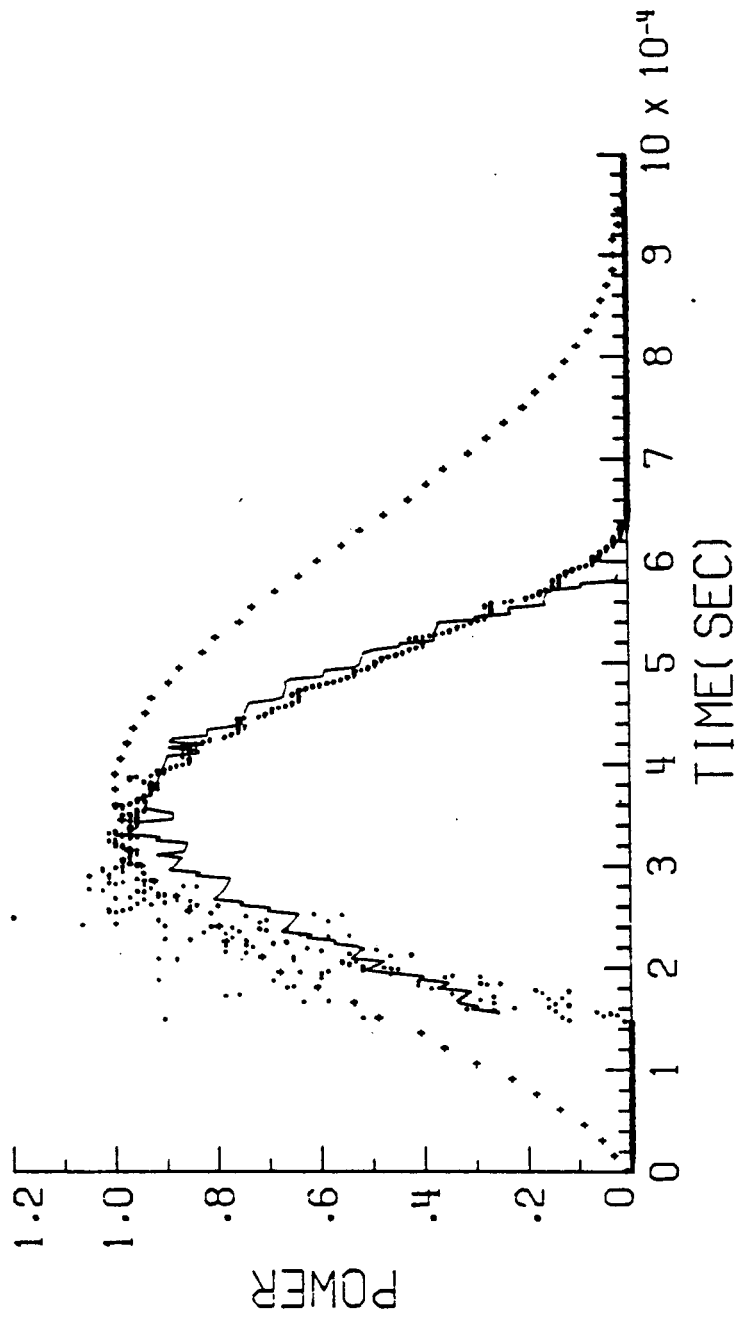


Figure 12

40 TORR

ALL PULSES NORMALIZED  
TO THEIR PEAK VALUE

— QUASI-STEADY STATE  
PULSE POWER DATA

+ LASER POWER DATA

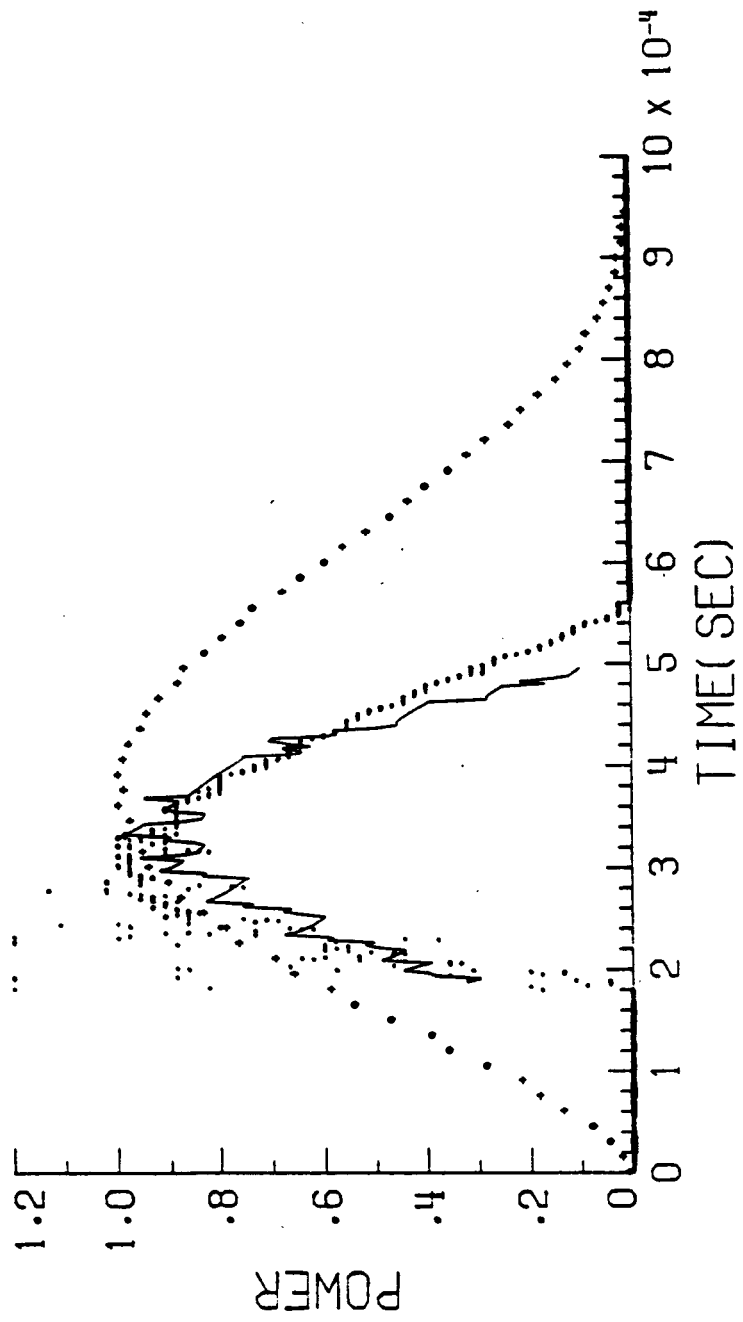


Figure 13

TABLE I. - MEAN REACTION RATE COEFFICIENTS AND ASSOCIATED  
UNCERTAINTY FACTORS BASED ON LITERATURE VALUES

The factor in parentheses gives the uncertainty limits associated  
with the coefficient.

Reactants	Products	Symbol	Reaction rate coefficient, (cm <sup>3</sup> )/sec R=i-C <sub>3</sub> F <sub>7</sub>
R + R	R <sub>2</sub>	K <sub>3</sub>	9.0 X 10 <sup>-13</sup> (3.8) <sup>+1</sup>
R + I	RI	K <sub>2</sub>	3.9 X 10 <sup>-11</sup> (4.3) <sup>+1</sup>
I + I +RI	I <sub>2</sub> + R	C <sub>2</sub>	3.7 X 10 <sup>-32</sup> (2.3) <sup>+</sup>
R + I*	RI	K <sub>1</sub>	1.7 X10 <sup>-13</sup> (17) <sup>+</sup>
I* + RI	I + RI	Q <sub>1</sub>	7 X 10 <sup>-17</sup> (4.1) <sup>+1</sup>
I* + I <sub>2</sub>	I + I <sub>2</sub>	Q <sub>2</sub>	3.1 x 10 <sup>-11</sup> (1.6) <sup>+1</sup>
I* + I + RI	I <sub>2</sub> + RI	C <sub>1</sub>	3.2 x 10 <sup>-33</sup> (3.2) <sup>+1</sup>

Table II Kinetic rate coefficient found to this date  
by numerical method for the two experiments.

Rate	Cylindrical Geometry	Rectangular Geometry
$K_1, \text{cm}^3/\text{s}$	$1.7 \times 10^{-13} (17)^{1.068}$	$1.7 \times 10^{-13} (17)^{.5512}$
$K_2, \text{cm}^3/\text{s}$	$3.9 \times 10^{-11} (4.3)^{-.3942}$	$3.9 \times 10^{-11} (4.3)^{-.0729}$
$K_3, \text{cm}^3/\text{s}$	$9.0 \times 10^{-13} (3.8)^{1.154}$	$9.0 \times 10^{-13} (3.8)^{.6614}$
$Q_1, \text{cm}^3/\text{s}$	$7.0 \times 10^{-17} (4.1)^{.3062}$	$7.0 \times 10^{-17} (4.1)^{-.0482}$
$Q_2, \text{cm}^3/\text{s}$	$3.1 \times 10^{-11} (1.6)^{1.0}$	$3.1 \times 10^{-11} (1.6)^{.5978}$
$C_1, \text{cm}^6/\text{s}$	$3.2 \times 10^{-33} (3.2)^{-.9289}$	$3.2 \times 10^{-33} (3.2)^{.5642}$
$C_2, \text{cm}^6/\text{s}$	$3.7 \times 10^{-32} (2.3)$	$3.7 \times 10^{-32} (2.3)$



Table III Data Set for Rectangular Resonator Laser Cavity (i-C<sub>3</sub>F<sub>7</sub>I)

Output Relative Peak Mirror Power (Max)	Total Pulse Energy(mJ)		Time to Threshold(mSec)		Lasing Time (mSec)	
	Experimental	Theoretical	Experimental	Theoretical	Experimental	Theoretical
.60	14.6	30.3	10.8	17.3	84	55
.50	7.06	11.1	16.0	27.6	84	35
.85	52.4	12.2	5.1	8.9	130	89
.85	23.0	6.8	6.2	10.4	182	88
.85	7.3	3.0	9.5	16.6	240	77

Table IV. Experimentnal data found in the previously reported  
 "Experiment on Perflouorobutyl Iodides as  
 Solar-Pumped Media for a Flashlamp-Pumped  
 Iodide Laser Oscillator System."

	Lasant Pressure(Torr)	Pulse Energy(J/cm <sup>2</sup> )	Threshold Time(us)	Lasing Time (us)
I-C <sub>3</sub> F <sub>7</sub> I	5	0.61	197	537
	10	1.23	167	528
	15	1.64	151	541
	20	1.85	151	519
	30	1.54	149	487
	40	1.83	179	367